Current amplification and relaxation in Dirac systems

Alexandra Junck,[1] Gil Refael,[2] and Felix von Oppen[1]
[1]*Dahlem Center for Complex Quantum Systems and Fachbereich Physik, Freie Universität Berlin, 14195 Berlin, Germany*
[2]*Department of Physics, California Institute of Technology, Pasadena, California 91125, USA*
(Received 14 January 2014; revised manuscript received 1 October 2014; published 2 December 2014)

Recent experiments provide evidence for photocurrent generation in Dirac systems such as topological-insulator surface states and graphene. Within the simplest picture, the magnitude of the photocurrents is governed by the competition between photoexcitation of particle-hole pairs and current relaxation by scattering. Here, we study the relaxation of photocurrents by electron-electron (*e*-*e*) collisions, which should dominate in clean systems. We compute the current relaxation rate as a function of the initial energies of the photoexcited carriers and the Fermi energy. For a positive Fermi energy, we find that collisions of a single excited electron with the Fermi sea can substantially increase the current, while for a single excited hole the current initially decreases. Together these processes partially cancel leading to a relative suppression of the relaxation of the total photocurrent carried by an electron-hole pair. We also analyze the limit of many scattering events and find that while *e*-*e* collisions initially reduce the current associated with a single hole, the current eventually reverses sign and becomes as large in magnitude as in the electron case. Thus, for photoexcited electron-hole pairs, the current ultimately relaxes to zero. We discuss schemes which may allow one to probe the nontrivial current amplification physics for individual carriers in experiment.

DOI: 10.1103/PhysRevB.90.245110 PACS number(s): 73.23.−b, 72.20.Jv, 73.20.At, 78.68.+m

I. INTRODUCTION

Dirac systems like graphene and topological insulators (TIs) are a central research topic in condensed-matter physics. The easy fabrication process of graphene [1] and the discovery of a variety of materials that are two dimensional (2D) [2–4] or 3D [5–8] TIs are but two reasons why Dirac systems are being intensively studied. Because of their linear dispersion and the associated helical (pseudo)spin structure, graphene and TIs might be valuable materials for spintronic devices [9]. In addition, graphene and TIs are promising systems for applications in the rising field of optoelectronics, for instance, as transparent conductors or photodetectors [10,11].

Photocurrents provide an interesting probe of the optoelectronic properties of Dirac materials and have been measured in both systems [12–16]. Their magnitude is governed by a competition between carrier excitation which is asymmetric in momentum space and current relaxation [17]. While there has been extensive research on energy relaxation of excited electrons both theoretically [18–26] and experimentally [27–34], current relaxation of photoexcited carriers in Dirac systems remains much less explored [15].

In this paper we provide a detailed account of the surprising process of current relaxation of highly excited carriers in Dirac materials. In general, current relaxation occurs through impurity, electron-phonon, or electron-electron (*e*-*e*) scattering. Here we study highly excited electrons, holes, and electron-hole pairs in the Dirac cone and assume that *e*-*e* interactions provide the dominant relaxation mechanism [see Fig. 2(a)] [22–25,32,35]. Interestingly, *e*-*e* scattering does not contribute to current relaxation when the carrier dispersion is quadratic. Indeed, for quadratic dispersions velocity is proportional to momentum and thus momentum conservation implies current conservation. In contrast, in Dirac systems with their linear dispersion, velocity is no longer proportional to momentum and the current can change and relax by *e*-*e* scattering [36].

In particular, such relaxation processes will cause relaxation of the current associated with a photoexcited particle-hole pair. Our results demonstrate that this relaxation process is highly asymmetric between electron and hole. In fact, the initial particle current gets amplified while the initial hole current is suppressed (assuming that the Fermi energy is above the Dirac point). As a result, we find that the current relaxation of zero-momentum p-h pairs is strongly suppressed due to cancellations between electron and hole processes. Specifically, in the limit of large excitation energies ϵ_1 of the initial carriers, the rate of change of both electron and hole currents varies linearly with ϵ_F/ϵ_1, but with opposite signs. These linear terms cancel in the relaxation of the photocurrent, which is therefore dominated by subleading contributions and scales as $\sim(\epsilon_F/\epsilon_1)^{3/2}$.

We also explain how the current amplification for a single initial carrier comes about, both in individual scattering events and after full (though momentum-conserving) equilibration by many collisions. Consider first a single excited electron above the Fermi sea. For a single scattering event, we find that the average change in current strongly depends on the position of the Fermi level, being positive for $\epsilon_F > 0$, and negative otherwise. In contrast, for an excited hole, a single scattering event increases the current when the Fermi energy lies below the Dirac point, but decreases it otherwise. The mean change of the current per scattering event is illustrated in Fig. 1 and is of the order of $\sim$10% for realistic parameters. Ultimately, these remarkable results can be traced back to the fact that at zero temperature, there is no current relaxation when the Fermi energy is right at the Dirac point.

The paper is organized as follows. In Sec. II we study the current relaxation in the limit of many scattering events. In Sec. III we look at the effect of individual scattering events of a single highly excited electron or hole and study the rate of change of the current in Sec. IV. We discuss implications for the observation of photocurrents and possible experimental signatures of the amplification effect in Sec. V before concluding in Sec. VI.

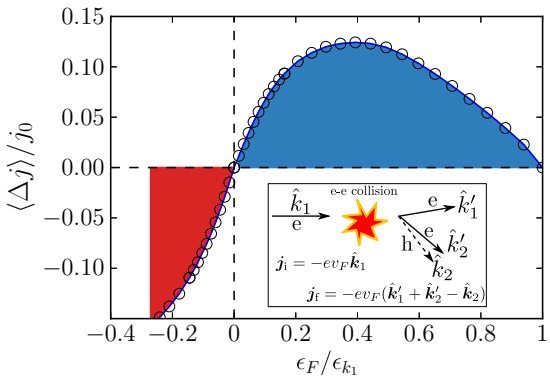

FIG. 1. (Color online) Mean change of the current per electron scattering event $\langle\Delta j\rangle/j_0$ relative to the initial current j_0 vs ϵ_F for fixed initial energy $\epsilon_{k_1} \approx 0.15$ eV. The blue and red shaded areas indicate current amplification and relaxation, respectively. The rate of change of the current is normalized by the total scattering rate Γ. The results are obtained for realistic parameters for Bi_2Se_3, including particle-hole asymmetry $\xi = 23.7$ eV Å^2, $v_F = 5 \times 10^5$ m/s [37], and $\alpha = 0.1$ (see text for definitions), where we assumed an average dielectric constant of air and Bi_2Se_3 of $\varepsilon \sim 50$ [38,39]. (Inset) Schematic of the excitation of an electron-hole pair by the initial photoexcited electron.

II. MANY SCATTERING EVENTS

It is perhaps easiest to demonstrate the intricacies of current relaxation due to *e-e* collisions in the limit of many collisions. Assume that relaxation is fully dominated by *e-e* scattering, and other scattering events, e.g., electron-phonon or electron-impurity scattering can be ignored. This limit is adequate in sufficiently clean samples (suppressed impurity scattering) at low temperatures (suppressed electron-phonon scattering). Then we can determine the resulting current after many scattering events on the basis of momentum conservation.

Consider first the photocurrent associated with photoexcited particle-hole pair. In this case, the initial photoexcited state has zero total momentum. Thus, the system relaxes to a Fermi distribution centered at zero momentum and the photocurrent ultimately relaxes back to zero. This seemingly obvious result actually comes about in a highly subtle manner when considering the current relaxation of the electron and the hole separately.

When an initially excited electron of energy $\epsilon_i > 0$ has completely relaxed, momentum conservation requires that its momentum will be distributed over the entire Fermi sea. For $\epsilon_F > 0$ the final current is thus given by

$$\boldsymbol{j}_f = -\frac{e\hbar v_F^2}{(2\pi)^2}\hat{\boldsymbol{k}}_i \int dk\, k \int d\phi \cos^2\phi \Delta k \delta(\epsilon - \epsilon_F), \qquad (1)$$

with $\Delta k = k_i/N$ the momentum shift per electron, $N = k_F^2 L^2/(4\pi)$ the number of electrons in the Fermi sea, and L^2 the system area. For a linear dispersion the initial current, i.e., the current before any *e-e* scattering events, is simply given by $\boldsymbol{j}_i = -ev_F\hat{\boldsymbol{k}}_i/L^2$ and the final current can be written as

$$\boldsymbol{j}_f = \frac{k_i}{k_F}\boldsymbol{j}_i. \qquad (2)$$

Thus, the current is amplified by a factor of $\epsilon_i/\epsilon_F > 1$ relative to the initial current carried by the initial excited electron.

In fact, the momentum-conservation argument is sufficiently general that we can study arbitrary power-law dispersions. Indeed, a straightforward extension of these considerations for a general dispersion $\epsilon \sim k^n$ yields $\boldsymbol{j}_f = \boldsymbol{j}_i(k_F/k_1)^{2-n}$, indicating that *e-e* scattering increases the current for $n < 2$ and decreases the current for $n > 2$. For quadratic dispersion, we have $\boldsymbol{j}_f = \boldsymbol{j}_i$, as expected, since momentum conservation implies current conservation in this case. This general result also implies that higher order corrections to the Dirac Hamiltonian, such as the cubic hexagonal warping, will reduce the amplification. In the case of warping ($\mathcal{H}_w \sim \lambda k^3\sigma_z$ for Bi_2Se_3), however, the correction will be of order λ^2 and thus small.

This argument can also be applied to the case of $\epsilon_F < 0$. With the same $\epsilon_i > 0$ as before, consider a chemical potential that is sufficiently negative such that after relaxation the conduction band of the Dirac system is completely empty. In this case momentum and velocity of the charge carriers are antiparallel. The final current actually flows in the direction opposite to the initial current and is also amplified in magnitude; i.e.,

$$\boldsymbol{j}_f^{(\epsilon_F<0)} = -\frac{k_i}{k_F}\boldsymbol{j}_i. \qquad (3)$$

We see below [cf. Eq. (13)] that this amplification of the current in the reverse direction will merely look like relaxation of the current when considering a single scattering event.

A simple extension of these considerations shows that the behavior of the initial hole is just inverted, with the hole current being amplified along the initial current direction for $\epsilon_F < 0$ and reversing sign for $\epsilon_F > 0$. Thus, for a photoexcited particle-hole pair, both the electron and the hole current actually *increase* in magnitude, albeit in opposite directions, causing overall photocurrent relaxation.

III. INDIVIDUAL SCATTERING EVENTS

The simplicity of the momentum conservation argument hides a rather subtle structure involving the current relaxation and amplification in Dirac systems. In the next two sections we take on the task of understanding how the effect emerges in single scattering events. This analysis is especially important for understanding the photocurrent response of Dirac materials. It is also important for energetic electrons (or holes) which relax partially through *e-e* interactions (following the cascade picture of Ref. [25]), but ultimately through momentum-nonconserving impurity or phonon scatterings.

The surprising possibility of an increase in current due to *e-e* scattering can be seen by analyzing the kinematic constraints of a single scattering process. Energy and momentum conservation demand

$$\epsilon_{\boldsymbol{k}_1} + \epsilon_{\boldsymbol{k}_2} = \epsilon_{\boldsymbol{k}'_1} + \epsilon_{\boldsymbol{k}'_2}, \qquad (4)$$

$$\boldsymbol{k}_1 + \boldsymbol{k}_2 = \boldsymbol{k}'_1 + \boldsymbol{k}'_2. \qquad (5)$$

Here $\boldsymbol{k}_i$ ($\boldsymbol{k}'_i$) is the momentum of the initial (final) electrons and $\epsilon_{\boldsymbol{k}} = \pm v_F k$ for the upper (conduction) and lower (valence) band, respectively. Expressed in terms of momentum, Eq. (4) depends on whether the specific scattering process is intraband or interband, with the allowed scattering processes depending on the Fermi energy.

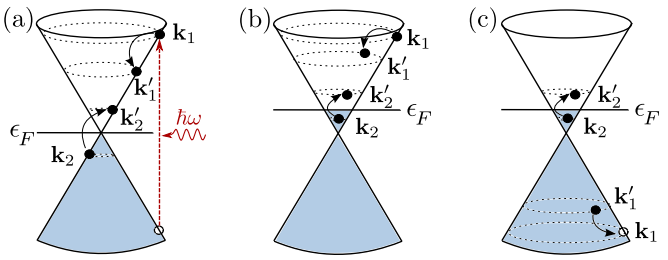

FIG. 2. (Color online) The photoexcitation of an electron-hole pair within the Dirac cone and the relaxation process of the hot electron by excitation of an electron-hole pair, for (a) $\epsilon_F = 0$ and (b) $\epsilon_F > 0$. (c) A possible relaxation process of the excited hole.

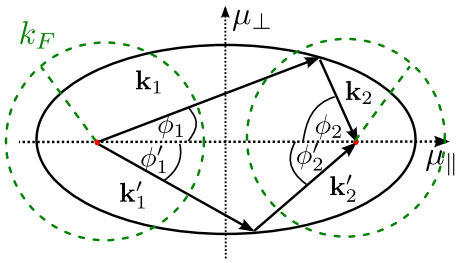

FIG. 3. (Color online) Kinematic ellipse for allowed electron scattering processes for $\epsilon_i > 0$. $\boldsymbol{k}_1$ and $\boldsymbol{k}_2$ are drawn head to tail starting and ending at the left and right focal points (red dots). $\boldsymbol{k}_1'$ and $\boldsymbol{k}_2'$ are drawn in a similar fashion and touch at points that lie on the ellipse. $(k_1 + k_2)/2$ and $|\boldsymbol{k}_1 + \boldsymbol{k}_2|$ are the lengths of the semimajor axis and the distance between focal points, respectively. The green dashed circle indicates the Fermi momentum. Because of Pauli's principle we have $k_2 \leqslant k_F < k_2', k_1'$ and the point where $\boldsymbol{k}_1'$ is connected to $\boldsymbol{k}_2'$ must lie on the ellipse outside the green dashed circles, while the point of connection of $\boldsymbol{k}_1$ and $\boldsymbol{k}_2$ has to lie inside the green dashed circle.

If the Fermi energy lies at the Dirac point, $\epsilon_F = 0$, a typical relaxation process of a highly excited electron is illustrated in Fig. 2(a). The excited electron relaxes by scattering off an electron in the Fermi sea, creating a hole in the valence band and an additional electron in the conduction band. Energy conservation [Eq. (4)] demands $k_1 - k_2 = k_1' + k_2'$, which takes into account that the electron in the Fermi sea has a negative energy, $\epsilon_{\boldsymbol{k}_2} = -v_F k_2$. Thus, the length of vector $\boldsymbol{k}_1$ must be equal to the sum of the lengths of the remaining three vectors. This is only satisfied for collinear scattering so that initial and final states have the same velocities, i.e., $\boldsymbol{v}_1 = \boldsymbol{v}_2 = \boldsymbol{v}_1' = \boldsymbol{v}_2'$, and the current remains unchanged in the *e-e* collision. For Dirac systems with the Fermi energy at the Dirac point, *e-e* interactions therefore do not relax current.

When the Fermi energy lies above the Dirac point, i.e., $\epsilon_F > 0$, the excited electron can interact with Fermi-sea electrons which are either in the conduction (+) or the valence (−) band [see Fig. 2(b)], corresponding to the processes $(+,+) \to (+,+)$ or $(+,-) \to (+,+)$. The previous argument for $\epsilon_F = 0$ implies that a collision with electrons in the valence band, $(+,-) \to (+,+)$, is collinear and does not relax current. Thus, we only need to consider intraband processes [see Fig. 2(b)]. Energy conservation, i.e., $k_1 + k_2 = k_1' + k_2'$ from Eq. (4), and momentum conservation (5) can now be graphically interpreted in terms of an ellipse as illustrated in Fig. 3. The energy $k_1 + k_2 = k_1' + k_2' = \text{const.}$ defines the semimajor axis, while $|\boldsymbol{k}_1 + \boldsymbol{k}_2| = |\boldsymbol{k}_1' + \boldsymbol{k}_2'|$ is the distance between the focal points.

This construction implies that the current actually increases along the direction of the initial current $\hat{\boldsymbol{k}}_1$. In a first step, we assume that not only $\boldsymbol{k}_1$ but also $\boldsymbol{k}_2$ is fixed. The resulting ellipse is defined by the axes $\hat{\mu}_\parallel(\boldsymbol{k}_2)$ and $\hat{\mu}_\perp(\boldsymbol{k}_2)$ (see Fig. 3). We show that a summation over all $\boldsymbol{k}_1'$ and $\boldsymbol{k}_2'$ restricted to the ellipse leads to a current increase along $\hat{\mu}_\parallel$, as well as a change in current along $\hat{\mu}_\perp$. In a second step, we sum over all $\boldsymbol{k}_2$, i.e., over all ellipses. It turns out that a possible change of the current along $\hat{\mu}_\perp$ averages to zero due to the rotational symmetry of the problem. Remarkably, the increase in current along $\hat{\mu}_\parallel$ averages to an increase along the direction of the initial current $\hat{\boldsymbol{k}}_1$ (see Appendix A).

The initial and final currents along $\hat{\mu}_\parallel$ are given by ($v_F = 1$, $e = 1$ for brevity)

$$j_\mathrm{i} = (\hat{\boldsymbol{k}}_1)_{\mu_\parallel} = \cos\phi_1, \tag{6}$$

$$j_\mathrm{f} = (\hat{\boldsymbol{k}}_1' + \hat{\boldsymbol{k}}_2' - \hat{\boldsymbol{k}}_2)_{\mu_\parallel} = \cos\phi_1' + \cos\phi_2' - \cos\phi_2, \tag{7}$$

where the angles are defined as in Fig. 3. To analyze the change in current, we have to compare $\cos\phi_1 + \cos\phi_2$ to $\cos\phi_1' + \cos\phi_2'$. It can be shown by elementary geometry that the sum of the cosines, restricted to the ellipse, has a maximum for the symmetric case where the point of connection of the corresponding vectors lies on $\hat{\mu}_\perp$ and falls off monotonically away from the maximum. We know from Pauli's principle that $k_2 \leqslant k_F < k_1', k_2'$. This implies that the point of connection of $\boldsymbol{k}_1$ and $\boldsymbol{k}_2$ must lie inside the green dashed circle of radius k_F, while the point of connection of $\boldsymbol{k}_1'$ and $\boldsymbol{k}_2'$ must lie outside this circle (see Fig. 3) and thus closer to the $\hat{\mu}_\perp$ axis. Hence, $j_\mathrm{f} \geqslant j_\mathrm{i}$ for any scattering event; i.e., the current increases along $\hat{\mu}_\parallel$. Averaging over $\boldsymbol{k}_2$, i.e., averaging over all ellipses, leads to an average increase of the current along $\boldsymbol{k}_1$ (see Appendix A). An analogous argument that shows that a single *e-e* scattering event decreases the current when $\epsilon_F < 0$ is given in Appendix A. Note, however, that the final current in the limit of many scattering events is also amplified for $\epsilon_F < 0$ but flows in the direction opposite to the initial current.

IV. QUANTITATIVE ANALYSIS

Quantitatively, the current relaxation rate for the optically excited electron-hole pair can be obtained within a golden-rule approach. For definiteness, we consider the surface states of the TI Bi_2Se_3, described by the (second-quantized) Dirac Hamiltonian

$$H = \sum_{\boldsymbol{k}} \Psi_{\boldsymbol{k}}^\dagger \mathcal{H}_{\boldsymbol{k}} \Psi_{\boldsymbol{k}} + \frac{1}{2} \sum_{\boldsymbol{q},\boldsymbol{k}_1,\boldsymbol{k}_2} \Psi_{\boldsymbol{k}_1+\boldsymbol{q}}^\dagger \Psi_{\boldsymbol{k}_2-\boldsymbol{q}}^\dagger V(\boldsymbol{q}) \Psi_{\boldsymbol{k}_2} \Psi_{\boldsymbol{k}_1}, \tag{8}$$

where $V(q) = e^2/2\varepsilon_0\varepsilon q$ is the Coulomb interaction and

$$\mathcal{H}_{\boldsymbol{k}} = v_F(k_x\sigma_y - k_y\sigma_x) \tag{9}$$

describes the single-particle Dirac dispersion with eigenenergies $\epsilon_{\boldsymbol{k}} = \pm v_F k$ and eigenstates $|\boldsymbol{k}_i\rangle$.

The initial photoexcitation creates an electron-hole pair with fixed momentum $\boldsymbol{k}_1$ [see Fig. 2(a)]. Then, the rate of change of the electron and hole currents is

$$\frac{d\boldsymbol{j}^{(e/h)}}{dt} = \mp e \sum_{\boldsymbol{k}_2,\boldsymbol{k}_1',\boldsymbol{k}_2'} (\boldsymbol{v}_1' + \boldsymbol{v}_2' - \boldsymbol{v}_1 - \boldsymbol{v}_2) W_{\boldsymbol{k}_1,\boldsymbol{k}_2;\boldsymbol{k}_1',\boldsymbol{k}_2'} \times f^{(e/h)}(\epsilon_{\boldsymbol{k}_2})\big[1 - f^{(e/h)}(\epsilon_{\boldsymbol{k}_1'})\big]\big[1 - f^{(e/h)}(\epsilon_{\boldsymbol{k}_2'})\big], \tag{10}$$

where the velocity is $\boldsymbol{v}_i = v_F \mathrm{sgn}(\epsilon_{\boldsymbol{k}_i})\hat{\boldsymbol{k}}_i$ and $f^{(e/h)}(\epsilon_{\boldsymbol{k}_i})$ denote the Fermi distribution function of electrons and holes, respectively. The transition rate is given by

$$W_{\boldsymbol{k}_1,\boldsymbol{k}_2;\boldsymbol{k}_1',\boldsymbol{k}_2'} = \frac{2\pi}{\hbar}|M|^2 \delta_{\boldsymbol{k}_1+\boldsymbol{k}_2,\boldsymbol{k}_1'+\boldsymbol{k}_2'} \delta(\epsilon_1 + \epsilon_2 - \epsilon_1' - \epsilon_2'), \tag{11}$$

with $\epsilon_i = \epsilon_{\boldsymbol{k}_i}$ and interaction matrix element

$$M = \frac{1}{2L^2}[\langle \boldsymbol{k}_1'|\boldsymbol{k}_1\rangle\langle \boldsymbol{k}_2'|\boldsymbol{k}_2\rangle u(|\boldsymbol{k}_1 - \boldsymbol{k}_1'|) - (\boldsymbol{k}_1' \leftrightarrow \boldsymbol{k}_2')]. \tag{12}$$

Here L^2 is the surface area of the system and $u(\boldsymbol{q}) = (e^2/2\varepsilon_0\varepsilon)/(q + q_{\mathrm{TF}})$ the screened Coulomb interaction, where $q_{\mathrm{TF}} = \alpha k_F$ is the Thomas-Fermi wave vector with $\alpha = e^2/(4\pi\hbar v_F \varepsilon_0 \varepsilon)$. As photoexcitation creates highly excited electron-hole pairs, we can set $T = 0$.

Equation (10) can be simplified by introducing the momentum transfer $\boldsymbol{q} = \boldsymbol{k}_1 - \boldsymbol{k}_1' = \boldsymbol{k}_2' - \boldsymbol{k}_2$ and the identity $\delta(\epsilon_1 + \epsilon_2 - \epsilon_1' - \epsilon_2') = \int d\omega \delta(\epsilon_1 - \epsilon_1' - \omega)\delta(\epsilon_2' - \epsilon_2 - \omega)$. Then, in the thermodynamic limit the two δ functions can be used to eliminate the angular integrals, leaving us with a 3D integral which can be solved numerically for general parameters and analytically in limiting cases (see Appendix C).

We first evaluate the expressions numerically for a particular carrier type, namely the photoexcited electron, and compute the mean change of current per scattering event. To make our results realistic, we include the particle-hole asymmetry of the dispersion through $\epsilon_{\boldsymbol{k}} = \pm v_F k + \xi k^2$ [40]. As illustrated in Fig. 1, for a single collision the current decreases for negative Fermi energies but becomes amplified for positive Fermi energies, with the current enhancement being of the order of $\sim$10%.

From now on, we assume a perfectly linear dispersion, i.e., $\xi = 0$, and $\epsilon_F > 0$ for definiteness. The case of negative Fermi energy follows by electron-hole symmetry. The rates of change of the electron, hole, and total currents, obtained by numerically integrating Eq. (10), are illustrated in the inset of Fig. 4. As already seen, for a single collision *e-e* scattering increases the electron current (red squares) and decreases the hole current (green diamonds). For large Fermi energies $\epsilon_F/\epsilon_1 \sim 1$ the rate of change approaches zero for the electron current and remains finite for the hole current, reflecting the different behavior of the phase space for scattering in the two cases [see Figs. 2(b) and 2(c)]. The *e-e* scattering also relaxes the total current (blue circles), but there are substantial cancellations between the electron and hole contributions. To quantify these cancellations, we analytically explore the asymptotic behavior of Eq. (10).

For the electron current, we only need to consider the scattering process illustrated in Fig. 2(b) because interband processes, i.e., $(+,-) \to (+,+)$, are collinear and do not change the current, as shown above by the geometric argument. For the hole, we have to consider scattering processes like the one illustrated in Fig. 2(c). The hole can recombine with an electron in the valence band, exciting an electron from the conduction band above the Fermi energy, i.e., $(-,+) \to (-,+)$, or the hole can recombine with an electron in the conduction band, exciting an electron from the valence band above the Fermi energy, i.e., $(-,+) \to (+,-)$. Other allowed processes will be collinear. We find that the asymptotic behavior of the rate of change of the electron and hole currents is given by

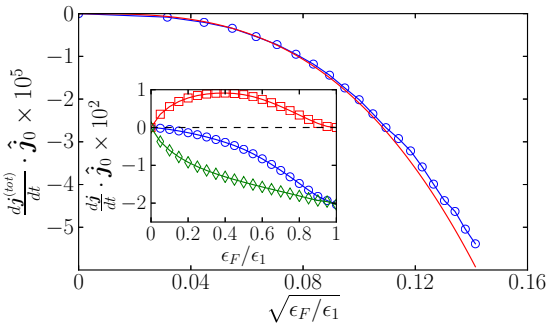

FIG. 4. (Color online) Rate of change of the total current (blue circles) [from Eq. (10)] and the asymptotic behavior $\sim(\epsilon_F/\epsilon_1)^{3/2}$ given by Eq. (14) (red). (Inset) Rates of change of the electron (red squares), hole (green diamonds), and total (blue circles) currents. Parameters as in Fig. 1. Relaxation of the total current is strongly suppressed due to cancellations between the electron and hole contributions. Results for $\epsilon_F < 0$ follow by electron-hole symmetry.

$$\frac{d\boldsymbol{j}^{(e/h)}}{dt} \approx \pm C\alpha^2 \frac{\epsilon_F}{\hbar}\boldsymbol{j}_0, \tag{13}$$

where $C \approx 0.3$ (see Appendix E), $\pm$ stands for the electron and hole current respectively, and $\boldsymbol{j}_0$ is the initial current of magnitude $j_0 = ev_F$ of the photoexcited carrier. This result has several interesting aspects. First, the time scale on which the initial current changes is independent of the large initial excitation energy ϵ_1 of the photoexcited carrier and instead depends on the Fermi energy only. This is a consequence of the fact that the typical energy transfer in the relevant *e-e* collisions is of the order of the Fermi energy. Second, to this order the rates of change of electron and hole currents differ only in their sign and thus cancel exactly. Thus, the rate of change of the total current of the photoexcited electron-hole pair is indeed much smaller and must scale with a higher power of ϵ_F/ϵ_1. We find that (see Appendix E)

$$\frac{d\boldsymbol{j}^{(\mathrm{tot})}}{dt} = \frac{d\boldsymbol{j}^{(e)}}{dt} + \frac{d\boldsymbol{j}^{(h)}}{dt} \approx -\frac{\alpha^2}{9}\frac{\epsilon_F}{\hbar}\left(\frac{\epsilon_F}{\epsilon_1}\right)^{1/2}\boldsymbol{j}_0. \tag{14}$$

The relaxation of the total current is suppressed for small ϵ_F/ϵ_1 and even vanishes in the limit $\epsilon_1 \to \infty$. Figure 4 shows the rate of change of the total current for small ϵ_F/ϵ_1 determined by numerically integrating Eq. (10) (blue circles) and the asymptotic behavior given by Eq. (14) (red solid line).

These asymptotic behaviors of the total current and the individual electron and hole currents can be traced back to distinct scattering processes. The amplification and relaxation of the individual currents are governed by scattering processes

with small energy transfers of the order of ϵ_F. In contrast, for the total current the contributions with small energy transfer cancel exactly to the order considered and the result in Eq. (14) arises solely from scattering processes with large energy transfers of the order of ϵ_1. Specifically, the relaxation of the total current is dominated by the interband hole process, $(-,+) \to (+,-)$, where the hole recombines with an electron from the conduction band while exciting an electron from the valence band to empty states in the conduction band. The predominance of scattering events with large energy transfers of the order of ϵ_1 also explains why the relaxation vanishes in the limit of $\epsilon_1 \to \infty$.

V. EXPERIMENTAL SIGNATURES OF THE AMPLIFICATION EFFECT

Aside from the important implications of this relaxation behavior for photocurrents, one might also want to search for direct signatures of the current amplification for single excited carriers. Finding clear signatures, however, could prove challenging. First, one needs to inject electrons of a certain energy and momentum into a Dirac system. One possible way to achieve this is based on momentum-conserving tunneling of electrons from a nanotube to graphene. An advantage of graphene over 3D TI is that graphene can be made remarkably clean and the 2D nature of graphene eliminates any unwanted bulk contributions.

Consider the setup illustrated in Fig. 5(a). An array of armchair nanotubes is placed above a graphene sheet, such that the nanotubes are parallel to the direction between the K and K' points of the graphene (i.e., parallel to a zigzag edge). The graphene sheet and the nanotube array can be gated independently and a bias applied between them. Then, the dispersion consists of two Dirac cones (one 1D and one 2D) which are shifted in energy as illustrated in Fig. 5(b). Assume that the Fermi energy of the graphene sheet is

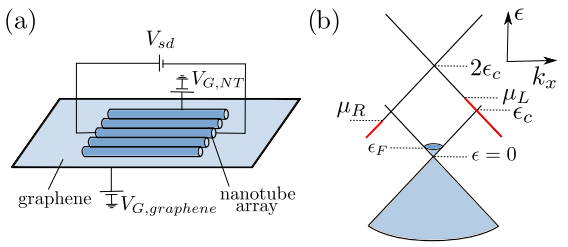

FIG. 5. (Color online) (a) Schematic illustration of the setup of a nanotube array on top of a graphene sheet. Using an array instead of a single nanotube might be advantageous in terms of gating, but, in principle, this effect also works for a single nanotube. The graphene sheet and the nanotube array will be gated independently with $V_{G,\text{graphene}}$ and $V_{G,NT}$ respectively, such that we have two shifted Dirac cones in momentum space as illustrated in part (b). The source-drain voltage V_{sd} leads to a bias between right movers and left movers in the nanotubes. (b) Two shifted Dirac cones for the nanotubes (top cone, 1D) and graphene (bottom, 2D), assuming that the nanotubes and graphene have the same Fermi velocity. The gate and source-drain voltages applied to the nanotubes should be adjusted such that $\mu_L > \epsilon_c > \mu_R$ so only, e.g., left-moving electrons can tunnel into graphene. The red color indicates occupied states in the nanotubes.

adjusted to a small, positive value and that an additional source-drain voltage is applied along the nanotube, inducing different chemical potentials for right and left movers in the nanotube. With proper adjustment of the gate and bias voltages, only, say, left-moving states in the nanotubes are occupied in the region where momentum-conserving tunneling is possible, as indicated by red color in Fig. 5(b). This requires that the nanotubes be sufficiently short such that there is no equilibration between left and right movers [41]. The tunneling electrons conserve the momentum component along the nanotube (say, the x direction), and the k_y component of the electronic momentum in graphene is adjusted to satisfy energy conservation. By symmetry, the current injected into the graphene sheet flows along the nanotube direction.

Even in this straightforward setup, the amplification measurement is subtle. The advantage of the system described is that the current tunneling from the nanotubes onto the graphene, translates in full to an opposite moving current of the same magnitude (this is not necessarily true given that tunneling may not generally result in unidirectionally moving electrons). Therefore, measuring the tunneling current yields also the prerelaxation current in the graphene. As it turns out, these statements are true even for tunneling into systems with nonlinear dispersion, as long as the tunneling process results in parallel-moving electrons. The linear dispersion differs, however, in how the current develops after injecting an electron pulse. For a quadratic dispersion, for instance, the current assumes its final value immediately after injection and is not affected by e-e scattering. For a linear dispersion, however, the current assumes its final value only after partial (energy) relaxation through e-e collisions, i.e., the final current is reached only after both the tunneling and relaxation steps take place. A ratio of the tunneling current to the measured current in the graphene, neglecting any resistances and relaxation processes due to the leads, should reveal the amplification effect. Furthermore, the bias and gate voltages, allow one to probe the dependence of the enhancement effect on the Fermi energy in graphene. This is particularly interesting because the ratio of injected to final current changes sign when tuning though the Dirac point. There is no analogous effect for a quadratic dispersion.

A time-resolved measurement may show an even more direct confirmation of our analysis. Given that the time scale for relaxation might be long relative to the tunneling time scale, a time-resolved measurement could also scrutinize the details of the amplification process. The necessary femtosecond time resolution has already been demonstrated in experiment on graphene [15,29,34].

We note that when scattering by impurities or phonons prevents the e-e interaction from fully relaxing the energy of an excited electron (or hole), the calculation of the current increase per collision can serve as an estimate of the current produced in a tunneling experiment. Particularly, e-e interactions make an energetic electron relax through a cascade of scattering processes that reduce the energy of the electron by roughly ϵ_F each [25]. The result displayed in Fig. 1 shows how each of these scattering events amplifies (or suppresses) the current. In a tunneling experiment as described above, if the non-Coulomb relaxation processes only allow $N < \epsilon_1/\epsilon_F$ e-e scattering events, with ϵ_1 the electron's initial energy, then the observed

current amplification effect in the Dirac system would be proportional to the sum of the amplification curve for electrons in Fig. 1 at values $\epsilon_F/\epsilon = \epsilon_F/(\epsilon_1 - n\epsilon_F)$ for $0 \leqslant n < N$.

VI. CONCLUSION

Motivated by photocurrent measurements on various Dirac systems, we investigated the interaction-induced relaxation of photocurrents in clean Dirac systems and uncovered a surprising effect: Due to cancellations between the electron and hole contributions, the current relaxation due to *e-e* scattering of photocurrents carried by electron-hole pairs is strongly suppressed. The reason is that for a chemical potential above the Dirac point, a single scattering event with the Fermi sea increases the current carried by the electron and decreases the current carried by the hole. In effect, both processes partially cancel.

There is a subtle point when comparing the scattering processes underlying energy and current relaxation. For a single excited electron or hole energy and current relaxation is governed by *e-e* scattering events with small energy transfer [25]. For a photoexcited electron-hole pair, however, the relaxation processes of the electron and hole cancel against each other to leading order, and the relaxation of the photocurrent is dominated by scattering events with large energy transfer, quite different from the energy relaxation picture. Our detailed analysis of the relaxation process shows that the initial relaxation rate of the photocurrent is proportional to $\epsilon_F^{3/2}$. The detailed results which we find for the Coulomb-induced relaxation process can also be combined with the cascade-relaxation picture [25] to determine the photocurrent response in the presence of various additional relaxation mechanisms, which are slower than the Coulomb processes but perhaps not slower than the complete momentum relaxation cascade.

The surprising underlying current increase which we find for a single collision of an excited electron when the chemical potential is above the Dirac point is quite substantial for realistic parameters. Once partial equilibrium is reached after many scattering events, the current is ultimately amplified by a factor of ϵ_1/ϵ_F. Strictly speaking, this amplification factor requires that other scattering processes can be neglected. It will be reduced when optical-phonon or impurity collisions compete, or when a large radiation intensity produces a high density of photoelectrons and phonons [24,25,42]. Thus, the amplification effect should be most pronounced for excited electrons with energies below optical-phonon frequencies ($\approx$200 meV for graphene) and for low-intensity irradiation.

Aside from the important implications for photocurrent measurements, we also discussed how to observe the amplification effect directly. We proposed an experimental setup that, by comparison of the measured final current with the theoretically calculated initial current, provides a way to study the amplification effect. In addition, the setup allows for strong gate control of the final current not only in magnitude but also in sign. A direct, all-experimental observation of the amplification in systems like graphene requires ultrafast time resolution which can nowadays be achieved with optical measurements [15,29,34]. One might also expect a strong nonlinear signature in IV characteristics, since high-energy electrons produce a jet of induced current. For the same reason, the current amplification might enhance the photoconductivity (electron conductivity in the presence of light), with the effect increasing with the frequency of the irradiating light. Other types of systems, e.g., cold atoms, might also hold promise for studying the amplification effect as they allow for tuning of the interactions.

ACKNOWLEDGMENTS

We thank J. Eisenstein, Erik Henriksen, Justin Song, Feng Wang, and Andrea Young for discussions and acknowledge financial support through SPP 1666 of the Deutsche Forschungsgemeinschaft and a Helmholtz Virtual Institute "New States of Matter and Their Excitations" (Berlin), as well as DARPA, the IQIM, an NSF institute supported by the Moore Foundation, and the Humboldt Foundation (Pasadena).

APPENDIX A: ANALYSIS OF KINEMATIC CONSTRAINTS

So far, we have shown that for an arbitrary $\boldsymbol{k}_2$ the component of the current along the direction given by the major axis of that specific ellipse, i.e., along $\hat{\mu}_\parallel(\boldsymbol{k}_2)$, increases due to *e-e* scattering. In general, the component of the current along $\hat{\mu}_\perp(\boldsymbol{k}_2)$ might also change during a scattering event. However, we still need to sum over all $\boldsymbol{k}_2$. Summing over $\boldsymbol{k}_2$ means summing over all possible ellipses and thus over all possible $\hat{\mu}_\parallel$ and $\hat{\mu}_\perp$. For a given $\boldsymbol{k}_2$ and resulting ϕ_1, by symmetry there is also a $\tilde{\boldsymbol{k}}_2$, i.e., the mirror image of $\boldsymbol{k}_2$ with respect to an axis parallel to $\boldsymbol{k}_1$, that leads to $-\phi_1$, as shown in Fig. 6. Thus, when summing over all possible $\boldsymbol{k}_2$, the increase of the component of the current along $\hat{\mu}_\parallel(\boldsymbol{k}_2)$ averages to a current increase along $\hat{\boldsymbol{k}}_1$. A change in the component along $\hat{\mu}_\perp(\boldsymbol{k}_2)$ has components parallel and perpendicular to $\boldsymbol{k}_1$. The component parallel to $\boldsymbol{k}_1$ changes sign under the described reflection and thus averages to zero. The component perpendicular to $\boldsymbol{k}_1$ also has to average to zero because the rotational symmetry of our systems requires that the average change in current can only be in the $\hat{\boldsymbol{k}}_1$ direction. By symmetry there can be no change in current perpendicular to $\hat{\boldsymbol{k}}_1$.

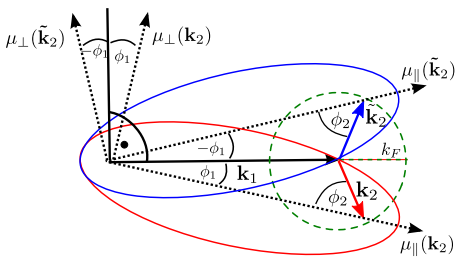

FIG. 6. (Color online) When averaging over all allowed $\boldsymbol{k}_2$, each $\boldsymbol{k}_2$ parametrizes a different ellipse. For each $\boldsymbol{k}_2$ and the resulting ellipse (red) there is a mirror image with respect to $\boldsymbol{k}_1$, $\tilde{\boldsymbol{k}}_2$ (blue), such that an increase in the current along $\hat{\mu}_\parallel(\boldsymbol{k}_2)$ averages to an increase along $\hat{\boldsymbol{k}}_1$. In general, there can also be a change of the current in direction $\hat{\mu}_\perp$. The change in the component parallel to $\boldsymbol{k}_1$, however, averages to zero when averaging over $\boldsymbol{k}_2$. By symmetry there can be no change in current perpendicular to $\boldsymbol{k}_1$. Changes of the current in the $\hat{\mu}_\perp$ direction are therefore not important for the average change in current. The green dashed circle indicates the Fermi momentum. The allowed states $\boldsymbol{k}_2$ must lie within this circle.

An analogous argument to the one presented here shows that e-e scattering decreases the current when $\epsilon_F < 0$.

APPENDIX B: DEFINITION OF THE MEAN CHANGE OF THE CURRENT PER ELECTRON SCATTERING EVENT

The mean change in current per scattering event is defined by

$$\frac{\langle \Delta j \rangle}{j_0} = \frac{1}{j_0 \Gamma}\frac{dj}{dt}. \tag{B1}$$

While dj/dt is always well defined, Γ diverges for a perfectly linear dispersion because the phase space for collinear scattering becomes infinite. We regularize this by introducing a physical and commonly used particle-hole asymmetry, such that $\epsilon_{\boldsymbol{k}} = \xi k^2 \pm v_F k$. When calculating the now well-defined Γ we have to take into account all allowed scattering processes. Processes that are collinear and can be neglected in the calculation of the rate of change of the current have to be included in Γ.

APPENDIX C: EVALUATION OF THE ENERGY-CONSERVATION δ FUNCTION

After introducing the momentum transfer $\boldsymbol{q} = \boldsymbol{k}_1 - \boldsymbol{k}_1' = \boldsymbol{k}_2' - \boldsymbol{k}_2$ the energy-conservation δ function can be written as

$$\begin{aligned}&\delta\left(\epsilon_{\boldsymbol{k}_1} + \epsilon_{\boldsymbol{k}_2} - \epsilon_{\boldsymbol{k}_1-\boldsymbol{q}} - \epsilon_{\boldsymbol{k}_2+\boldsymbol{q}}\right)\\ &\quad = \frac{1}{\hbar v_F}\int dp\,\delta(k_1 - |\boldsymbol{k}_1 - \boldsymbol{q}| - p)\delta(|\boldsymbol{k}_2 + \boldsymbol{q}| - k_2 - p),\end{aligned} \tag{C1}$$

where $\hbar v_F p$ is the difference in energy of the initial and final scattering states. Using the relation $\delta(a-b) = 2a\delta(a^2 - b^2)$, with $a, b > 0$, we can write

$$\begin{aligned}&\delta(k_1 - |\boldsymbol{k}_1 - \boldsymbol{q}| - p)\\ &\quad = 2(k_1 - p)\delta((k_1 - p)^2 - |\boldsymbol{k}_1 - \boldsymbol{q}|^2)\\ &\quad = 2(k_1 - p)\int_0^{2\pi} d\phi_q\, f(\cos\phi_q)\\ &\qquad \times\delta(-2k_1 p + p^2 - q^2 + 2k_1 q\cos\phi_q)\\ &\quad = \frac{(k_1 - p)}{k_1 q}\delta\left(\cos\phi_q - \frac{q^2 - p^2 + 2k_1 p}{2k_1 q}\right)\\ &\qquad \times\theta\left(1 - \left|\frac{q^2 - p^2 + 2k_1 p}{2k_1 q}\right|\right),\end{aligned} \tag{C2}$$

where ϕ_q is the angle between $\boldsymbol{k}_1$ and $\boldsymbol{q}$, such that

$$\begin{aligned}&\int_0^{2\pi} d\phi_q\, f(\cos\phi_q)\delta(k_1 - |\boldsymbol{k}_1 - \boldsymbol{q}| - p)\\ &\quad = 2\frac{(k_1 - p)}{k_1 q}\frac{f\left(\frac{q^2 - p^2 + 2k_1 p}{2k_1 q}\right)}{\sqrt{1 - \left(\frac{q^2 - p^2 + 2k_1 p}{2k_1 q}\right)^2}}\theta\\ &\qquad \times\left(1 - \left|\frac{q^2 - p^2 + 2k_1 p}{2k_1 q}\right|\right),\end{aligned} \tag{C3}$$

where the factor of 2 comes from the fact that $\cos\phi - a$ has two zeros in the interval $[0, 2\pi]$, with $|a| \leqslant 1$. Analogously, the ϕ_2 integration can be performed evaluating $\delta(|\boldsymbol{k}_2 + \boldsymbol{q}| - k_2 - p)$.

APPENDIX D: IDENTIFICATION OF DISTINCT SCATTERING PROCESSES IN THE ASYMPTOTIC BEHAVIOR OF THE RATE OF CHANGE OF THE CURRENT

For $\epsilon_F > 0$ we only need to consider processes like the one illustrated in Fig. 7(a), in which the excited electron scatters off an electron in the upper band. Other allowed processes will be collinear and thus do not change the current. The rate of change of the electron current is then given by

$$\begin{aligned}\frac{d\boldsymbol{j}^e}{dt} &= -e\frac{1}{4L^4}\frac{2\pi}{\hbar}\left(\frac{e^2}{2\epsilon_0\epsilon}\right)^2 \sum_{\boldsymbol{k}_2,\boldsymbol{k}_2',\boldsymbol{k}_1'} \delta\left(\epsilon_{\boldsymbol{k}_1} + \epsilon_{\boldsymbol{k}_2} - \epsilon_{\boldsymbol{k}_1'} - \epsilon_{\boldsymbol{k}_2'}\right)\\ &\quad\times(\hat{\boldsymbol{k}}_1' + \hat{\boldsymbol{k}}_2' - \hat{\boldsymbol{k}}_1 - \hat{\boldsymbol{k}}_2)\\ &\quad\times\left|\frac{\langle \boldsymbol{k}_1, +|\boldsymbol{k}_1', +\rangle\langle \boldsymbol{k}_2, +|\boldsymbol{k}_2', +\rangle}{|\boldsymbol{k}_1 - \boldsymbol{k}_1'| + q_{\mathrm{TF}}}\right.\\ &\quad\left. - \frac{\langle \boldsymbol{k}_1, +|\boldsymbol{k}_2', +\rangle\langle \boldsymbol{k}_2, +|\boldsymbol{k}_1', +\rangle}{|\boldsymbol{k}_1 - \boldsymbol{k}_2'| + q_{\mathrm{TF}}}\right|^2\\ &\quad\times\theta\left(\epsilon_F - \epsilon_{\boldsymbol{k}_2}\right)\theta\left(\epsilon_{\boldsymbol{k}_2'} - \epsilon_F\right)\theta\left(\epsilon_{\boldsymbol{k}_1'} - \epsilon_F\right)\\ &= -e\frac{1}{4L^4}\frac{2\pi}{\hbar}\left(\frac{e^2}{2\epsilon_0\epsilon}\right)^2 \sum_{\boldsymbol{k}_2,\boldsymbol{k}_2',\boldsymbol{k}_1'} \delta\left(\epsilon_{\boldsymbol{k}_1} + \epsilon_{\boldsymbol{k}_2} - \epsilon_{\boldsymbol{k}_1'} - \epsilon_{\boldsymbol{k}_2'}\right)\\ &\quad\times(\hat{\boldsymbol{k}}_1' + \hat{\boldsymbol{k}}_2' - \hat{\boldsymbol{k}}_1 - \hat{\boldsymbol{k}}_2)\left(\left|M_d^e - M_{\mathrm{ex}}^e\right|^2\right)\\ &\quad\times\theta\left(\epsilon_F - \epsilon_{\boldsymbol{k}_2}\right)\theta\left(\epsilon_{\boldsymbol{k}_2'} - \epsilon_F\right)\theta\left(\epsilon_{\boldsymbol{k}_1'} - \epsilon_F\right),\end{aligned} \tag{D1}$$

where the sum is over states with positive energy only and we decide to call the first term in the interaction matrix element "direct" and the second "exchange." Performing the sum, we find that the contributions to the rate of change from $|M_d^e|^2$ and $|M_{\mathrm{ex}}^e|^2$ are equal, as can be easily seen by switching the labels $\boldsymbol{k}_1' \leftrightarrow \boldsymbol{k}_2'$ in one of the terms. We call these contributions $d\boldsymbol{j}_d^e/dt$ and $d\boldsymbol{j}_{\mathrm{ex}}^e/dt$, respectively, with $d\boldsymbol{j}_d^e/dt = d\boldsymbol{j}_{\mathrm{ex}}^e/dt$. The remaining contribution from the interference term proportional to $2\mathrm{Re}[M_d^e(M_{\mathrm{ex}}^e)^*]$ we call $d\boldsymbol{j}_{\mathrm{inter}}^e/dt$.

Analogously for the hole current, we only need to consider processes where the hole recombines with an electron in the lower (upper) band, thereby exciting an electron from the upper (lower) band above the Fermi energy; i.e., the states $|\boldsymbol{k}_1'\rangle$, $|\boldsymbol{k}_2'\rangle$ of the scattering event are in different bands, as illustrated in Fig. 7(b). Processes where $|\boldsymbol{k}_1'\rangle$, $|\boldsymbol{k}_2'\rangle$ are in the same band

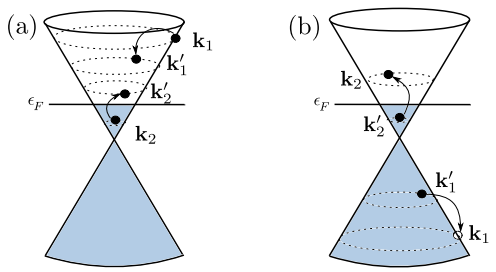

FIG. 7. (Color online) (a) Electron and (b) hole process for the case of $\epsilon_F > 0$. (a) Scattering processes where $|\boldsymbol{k}_2\rangle$ is in the lower band are collinear and will not change the current. (b) Processes where $|\boldsymbol{k}_1'\rangle$, $|\boldsymbol{k}_2'\rangle$ are in the same band are also collinear.

are collinear and thus do not change the current. The rate of change of the hole current can be written as

$$\begin{aligned}\frac{d\boldsymbol{j}^h}{dt} &= 2e\frac{1}{4L^4}\frac{2\pi}{\hbar}\left(\frac{e^2}{2\epsilon_0\epsilon}\right)^2\sum_{\boldsymbol{k}_2,\boldsymbol{k}_2',\boldsymbol{k}_1'}\delta\left(\epsilon_{\boldsymbol{k}_1}+\epsilon_{\boldsymbol{k}_2}-\epsilon_{\boldsymbol{k}_1'}-\epsilon_{\boldsymbol{k}_2'}\right)\\ &\times(-\hat{k}_1'+\hat{k}_2'+\hat{k}_1-\hat{k}_2)\\ &\times\left|\frac{\langle\boldsymbol{k}_1,-|\boldsymbol{k}_1'|,-\rangle\langle\boldsymbol{k}_2,+|\boldsymbol{k}_2'|,+\rangle}{|\boldsymbol{k}_1-\boldsymbol{k}_1'|+q_{\mathrm{TF}}}\right.\\ &\left.-\frac{\langle\boldsymbol{k}_1,-|\boldsymbol{k}_2'|,+\rangle\langle\boldsymbol{k}_2,+|\boldsymbol{k}_1'|,-\rangle}{|\boldsymbol{k}_1-\boldsymbol{k}_2'|+q_{\mathrm{TF}}}\right|^2\\ &\times\theta\left(\epsilon_{\boldsymbol{k}_2}-\epsilon_F\right)\theta\left(\epsilon_F-\epsilon_{\boldsymbol{k}_2'}\right)\\ &= 2e\frac{1}{4L^4}\frac{2\pi}{\hbar}\left(\frac{e^2}{2\epsilon_0\epsilon}\right)^2\sum_{\boldsymbol{k}_2,\boldsymbol{k}_2',\boldsymbol{k}_1'}\delta\left(\epsilon_{\boldsymbol{k}_1}+\epsilon_{\boldsymbol{k}_2}-\epsilon_{\boldsymbol{k}_1'}-\epsilon_{\boldsymbol{k}_2'}\right)\\ &\times(-\hat{k}_1'+\hat{k}_2'+\hat{k}_1-\hat{k}_2)\\ &\times\left(\left|M_d^h-M_{\mathrm{ex}}^h\right|^2\right)\theta\left(\epsilon_{\boldsymbol{k}_2}-\epsilon_F\right)\theta\left(\epsilon_F-\epsilon_{\boldsymbol{k}_2'}\right),\end{aligned}\tag{D2}$$

where we restricted the sum to $\epsilon_{\boldsymbol{k}_1'}<0$ and $\epsilon_{\boldsymbol{k}_2'}>0$ and added the factor of 2 in front for the other half of the sum. We again call the first term of the interaction matrix element "direct" and the second "exchange." Analogously to above, we call the corresponding contributions to the rate of change of the hole current $d\boldsymbol{j}_d^h/dt$ and $d\boldsymbol{j}_{\mathrm{ex}}^h/dt$, and $d\boldsymbol{j}_{\mathrm{inter}}^h/dt$. Here the contributions from direct and exchange term are not equal because the states $|\boldsymbol{k}_1'\rangle$, $|\boldsymbol{k}_2'\rangle$ are in different bands. Switching the labels as for the electron current does not transform one term into the other.

For large excitation energies, i.e., for $\epsilon_F/\epsilon_1\ll 1$, we find to lowest order that

$$\frac{d\boldsymbol{j}_d^e}{dt}+\frac{d\boldsymbol{j}_{\mathrm{ex}}^e}{dt}\approx-\frac{d\boldsymbol{j}_d^h}{dt},\tag{D3}$$

$$\frac{d\boldsymbol{j}_{\mathrm{inter}}^e}{dt}\approx-\frac{d\boldsymbol{j}_{\mathrm{inter}}^e}{dt}.\tag{D4}$$

As shown in the next section, this cancellation results in the fact that the rate of change of the total current to leading order is simply given by

$$\frac{d\boldsymbol{j}^{\mathrm{tot}}}{dt}=\frac{d\boldsymbol{j}^e}{dt}+\frac{d\boldsymbol{j}^h}{dt}\approx\frac{d\boldsymbol{j}_{\mathrm{ex}}^h}{dt}.\tag{D5}$$

$d\boldsymbol{j}_{\mathrm{ex}}^h/dt$ is governed by the interaction matrix element

$$\left|M_{\mathrm{ex}}^h\right|^2=\left|\frac{\langle\boldsymbol{k}_1,-|\boldsymbol{k}_2'|,+\rangle\langle\boldsymbol{k}_2,+|\boldsymbol{k}_1'|,-\rangle}{|\boldsymbol{k}_1-\boldsymbol{k}_2'|+q_{\mathrm{TF}}}\right|^2,\tag{D6}$$

which describes processes where the photoexcited hole recombines with an electron from the upper band, thereby exciting an electron from the lower band above the Fermi energy. These scattering processes involve large energy transfers of the order of the initial excitation energy ϵ_1.

APPENDIX E: ASYMPTOTIC BEHAVIOR OF THE RATE OF CHANGE OF THE CURRENT FOR LARGE EXCITATION ENERGIES

We now want to calculate the asymptotic behavior of the rates of change of the individual electron and hole currents and of the total current. We show the calculation for $d\boldsymbol{j}_d^e/dt$ in detail. The calculations of the remaining contributions follow analogously.

After introducing the momentum transfer $\boldsymbol{q}=\boldsymbol{k}_1-\boldsymbol{k}_1'=\boldsymbol{k}_2'-\boldsymbol{k}_2$, we use that the Coulomb interaction in the direct term of Eq. (D1) is proportional to $\sim 1/(q+q_{\mathrm{TF}})$ and the integral will be dominated by scattering events with small momentum transfer $q\ll k_1$. We now fix the initial momentum of the excited electron-hole pair $\boldsymbol{k}_1=k_1\hat{x}$ such that the initial current is given by $\boldsymbol{j}_0=-2ev\hat{x}$. The difference of the velocities of states $\boldsymbol{k}_1$ and $\boldsymbol{k}_1'$ can be approximated by zero; i.e.,

$$\hat{k}_1'-\hat{k}_1=\frac{k_1-q\cos\phi_q}{|\boldsymbol{k}_1-\boldsymbol{q}|}-1\approx 0.\tag{E1}$$

We can also approximate the spin overlap of states $\boldsymbol{k}_1$ and $\boldsymbol{k}_1'$ by 1; i.e.,

$$|\langle\boldsymbol{k}_1|\boldsymbol{k}_1'\rangle|^2=\frac{k_1-q\cos\phi_q+|\boldsymbol{k}_1-\boldsymbol{q}|}{2|\boldsymbol{k}_1-\boldsymbol{q}|}\approx 1.\tag{E2}$$

The initial current flows in the negative x direction so the rate of change of the current will only have an x component. By the rotational symmetry of our problem there can be no change of the current along $\hat{y}$. The sum of the quadratic direct and exchange contributions to the rate of change of the electron current given by Eq. (D1) can then be written as

$$\begin{aligned}\frac{dj_d^e}{dt}+\frac{dj_{\mathrm{ex}}^e}{dt} &= -ev\frac{1}{2L^4}\frac{2\pi}{\hbar}\left(\frac{e^2}{2\epsilon_0\epsilon}\right)^2\sum_{\boldsymbol{k}_2,\boldsymbol{q}}\frac{1}{\hbar v}\delta(k_1+k_2-|\boldsymbol{k}_1-\boldsymbol{q}|-|\boldsymbol{k}_2+\boldsymbol{q}|)\\ &\times\left[\frac{k_2\cos(\phi_2+\phi_q)+q\cos\phi_q}{|\boldsymbol{k}_2+\boldsymbol{q}|}-\cos(\phi_2+\phi_q)\right]\left[\frac{k_2+q\cos\phi_2+|\boldsymbol{k}_2+\boldsymbol{q}|}{2|\boldsymbol{k}_2+\boldsymbol{q}|(q+\alpha k_F)^2}\right]\theta(k_F-k_2)\theta(|\boldsymbol{k}_2+\boldsymbol{q}|-k_F),\end{aligned}\tag{E3}$$

where $\alpha=e^2/(4\pi\hbar v_F\varepsilon_0\varepsilon)$ is defined by $q_{\mathrm{TF}}=\alpha k_F$. As above, we use the identity

$$\delta(k_1+k_2-|\boldsymbol{k}_1-\boldsymbol{q}|-|\boldsymbol{k}_2+\boldsymbol{q}|)=\int dp\,\delta(k_1-|\boldsymbol{k}_1-\boldsymbol{q}|-p)\delta(|\boldsymbol{k}_2+\boldsymbol{q}|-k_2-p)\tag{E4}$$

and evaluate the ϕ_2 and ϕ_q integrations with the two δ functions as shown in Eqs. (C2) and (C3). In Eq. (E3), however, we not only have terms with $\cos\phi_2$ and $\cos\phi_q$ but also terms that contain $\sin\phi_2 \sin\phi_q$. Depending on the values of ϕ_2 and ϕ_q, we can write

$$\sin\phi_2 \sin\phi_q = \pm\sqrt{1-\cos^2\phi_2}\sqrt{1-\cos^2\phi_q}. \tag{E5}$$

Since we have to integrate both ϕ_2 and ϕ_q from 0 to 2π, integration of the terms proportional to $\sin\phi_2 \sin\phi_q$ gives zero. Thus, in the integrand of Eq. (E3) we can neglect the terms proportional to $\sin\phi_2 \sin\phi_q$, leaving us with a function that only depends on $\cos\phi_2$ and $\cos\phi_q$. Performing the ϕ_2 and ϕ_q integrations using Eq. (C3) and simplifying the result, we are left with

$$\begin{aligned}\frac{dj_d^e}{dt} + \frac{dj_{\rm ex}^e}{dt} = -ev\frac{1}{2}\frac{2\pi}{\hbar}\left(\frac{e^2}{2\epsilon_0\epsilon}\right)^2 \frac{1}{\hbar v}\frac{1}{(2\pi)^4}\left(\int_0^{k_F} dp \int_{k_F-p}^{k_F} dk_2 + \int_{k_F}^{k_1-k_F} dp \int_0^{k_F} dk_2\right)\int_p^{2k_2+p} dq \\ \times (k_1-p)\frac{\sqrt{(2k_2+p)^2-q^2}}{\sqrt{(2k_1-p)^2-q^2}}\left(\frac{q^2-p^2+2k_1p}{k_1q}\right)\frac{1}{(q+\alpha k_F)^2}\frac{(2k_2+p)}{k_2(k_2+p)}.\end{aligned} \tag{E6}$$

For the integral over small $p \ll k_1$ we can approximate the integrand further. Introducing dimensionless parameters $\bar{p} = p/k_F$, $\bar{q} = q/k_F$, and $\bar{k_2} = k_2/k_F$ and shifting the integration variable $k_2 \to k_2 + p/2$, we get

$$-\frac{D}{4\pi}\frac{\epsilon_F}{\epsilon_1}\int_0^1 d\bar{p}\int_{1-\bar{p}/2}^{1+\bar{p}/2} d\bar{k_2}\int_{\bar{p}}^{2\bar{k_2}} d\bar{q}\sqrt{(2\bar{k_2})^2-\bar{q}^2}\left(\frac{\bar{p}}{\bar{q}}\right)\frac{1}{(\bar{q}+\alpha)^2}\frac{2\bar{k_2}}{\bar{k_2}^2-\frac{\bar{p}^2}{4}} \approx -\gamma\frac{D}{4\pi}\frac{\epsilon_F}{\epsilon_1}, \tag{E7}$$

with $\gamma \approx 1.17$ from numerical integration and $D = ev_F\alpha^2\epsilon_1/\hbar$ and $\alpha = 0.1$ as in the main text.

For the remaining integral we also use the dimensionless parameters $\bar{p}$, $\bar{q}$, and $\bar{k_2}$. If the integral converges, then the integrand has to go to zero faster than $1/p$; i.e., the weight is negligible for large p and we are still allowed to approximate $p \ll k_1$. The integral becomes

$$-\frac{D}{4\pi}\frac{\epsilon_F}{\epsilon_1}\int_1^{k_1/k_F-1} dp\int_0^1 d\bar{k_2}\int_{\bar{p}}^{2\bar{k_2}+\bar{p}} dq\sqrt{2p}\sqrt{2\bar{k_2}+\bar{p}-\bar{q}}\left(\frac{\bar{p}}{\bar{q}}\right)\frac{1}{(\bar{q}+\alpha)^2}\frac{(2\bar{k_2}+\bar{p})}{\bar{k_2}(\bar{k_2}+\bar{p})}. \tag{E8}$$

We are interested in the limit $k_1/k_F \to \infty$. To avoid numerical integration up to infinity we use that for the region $p \gg k_2$ we can approximate $p \approx q$ and get

$$I_> = -\frac{D}{4\pi}\frac{\epsilon_F}{\epsilon_1}\int_\Lambda^\infty d\bar{p}\int_0^1 d\bar{k_2}\int_{\bar{p}}^{2\bar{k_2}+\bar{p}} d\bar{q}\sqrt{2\bar{p}}\sqrt{2\bar{k_2}+\bar{p}-\bar{q}}\frac{1}{\bar{p}^2}\frac{1}{\bar{k_2}} = -\frac{D}{4\pi}\frac{8}{3}\frac{2}{3}\frac{\epsilon_F}{\epsilon_1}\int_\Lambda^\infty d\bar{p}\frac{1}{\bar{p}^{3/2}}, \tag{E9}$$

where Λ is a cutoff that ensures that the approximation $p \gg k_2$ is valid. The remaining part of the integral we cannot approximate further and we have to integrate

$$I_< = -\frac{D}{4\pi}\frac{\epsilon_F}{\epsilon_1}\int_1^\Lambda d\bar{p}\int_0^1 d\bar{k_2}\int_{\bar{p}}^{2\bar{k_2}+\bar{p}} d\bar{q}\sqrt{2\bar{p}}\sqrt{2\bar{k_2}+\bar{p}-\bar{q}}\left(\frac{\bar{p}}{\bar{q}}\right)\frac{1}{(\bar{q}+\alpha)^2}\frac{(2\bar{k_2}+\bar{p})}{\bar{k_2}(\bar{k_2}+\bar{p})} \tag{E10}$$

numerically. For $\Lambda = 10$ we get $I_> = -\frac{16}{9}\sqrt{2/5}D/(4\pi)(\epsilon_F/\epsilon_1)$ and $I_< \approx -1.93D/(4\pi)(\epsilon_F/\epsilon_1)$ and for $\Lambda = 100$ we get $I_> = -\frac{16}{9}\frac{1}{5}D/(4\pi)(\epsilon_F/\epsilon_1)$ and $I_< \approx -2.68D/(4\pi)(\epsilon_F/\epsilon_1)$. Both cutoffs give us the same final result of

$$\frac{d\boldsymbol{j}_d^e}{dt} + \frac{dj_{\rm ex}^e}{dt} \approx 4.2\frac{D}{4\pi}\frac{\epsilon_F}{\epsilon_1}\hat{j}_0 \approx 0.3ev_F\alpha^2\frac{\epsilon_F}{\hbar}\hat{j}_0. \tag{E11}$$

An analogous calculation for the interference term shows that $\frac{dj_{\rm inter}^e}{dt} \sim -D/(4\pi)(\epsilon_F/\epsilon_1)^{3/2}$, which is of higher order.

It can be easily shown that to lowest order in ϵ_F/ϵ_1, $(dj_d^e/dt) + (dj_{\rm ex}^e/dt)$ and (dj_d^h/dt) just differ by a sign. In Fig. 7(b), labeling the initial states by $\boldsymbol{k}_1$, $\boldsymbol{k}_2'$ and the final states by $\boldsymbol{k}_1'$, $\boldsymbol{k}_2$, i.e., switching $\boldsymbol{k}_2 \leftrightarrow \boldsymbol{k}_2'$, and making use of the approximations (E1) and (E2), the direct term of the hole current can be written as

$$\frac{d\boldsymbol{j}_d^h}{dt} \approx 2e\frac{1}{4L^4}\frac{2\pi}{\hbar}\left(\frac{e^2}{2\epsilon_0\epsilon}\right)^2\sum_{\boldsymbol{k}_2,\boldsymbol{k}_2',\boldsymbol{k}_1'}\delta\big(\epsilon_{\boldsymbol{k}_1}+\epsilon_{\boldsymbol{k}_2'}-\epsilon_{\boldsymbol{k}_1'}-\epsilon_{\boldsymbol{k}_2}\big)(\hat{k}_2-\hat{k}_2')\left|\frac{\langle\boldsymbol{k}_2',+|\boldsymbol{k}_2,+\rangle}{|\boldsymbol{k}_1-\boldsymbol{k}_1'|+q_{\rm TF}}\right|^2\theta\big(\epsilon_{\boldsymbol{k}_2'}-\epsilon_F\big)\theta\big(\epsilon_F-\epsilon_{\boldsymbol{k}_2}\big), \tag{E12}$$

where $\boldsymbol{k}_2' = \boldsymbol{k}_2 - \boldsymbol{q}$. The transformation $\phi_2 \to \phi_2 + \pi$ leads to $\boldsymbol{k}_2 \to -\boldsymbol{k}_2$ and $\boldsymbol{k}_2 - \boldsymbol{q} \to -(\boldsymbol{k}_2 + \boldsymbol{q})$. With $|-\boldsymbol{k},\pm\rangle = |\boldsymbol{k},\mp\rangle$ and $|\langle\boldsymbol{k},+|\boldsymbol{k}',+\rangle|^2 = |\langle\boldsymbol{k},-|\boldsymbol{k}',-\rangle|^2$, we find to lowest order that

$$\frac{d\boldsymbol{j}_d^h}{dt} = -\left(\frac{d\boldsymbol{j}_d^e}{dt} + \frac{d\boldsymbol{j}_{\rm ex}^e}{dt}\right). \tag{E13}$$

Analogous calculations to the one above for dj_d^e/dt lead to

$$\begin{aligned}
\frac{d\boldsymbol{j}^e_{\text{inter}}}{dt} &\sim \frac{D}{4\pi}\left(\frac{\epsilon_F}{\epsilon_1}\right)^{3/2}\hat{j}_0,\\
\frac{d\boldsymbol{j}^h_{\text{inter}}}{dt} &\sim -\frac{D}{4\pi}\left(\frac{\epsilon_F}{\epsilon_1}\right)^{3/2}\hat{j}_0,\\
\frac{d\boldsymbol{j}^e_{\text{inter}}}{dt}+\frac{d\boldsymbol{j}^h_{\text{inter}}}{dt} &\sim -\frac{D}{4\pi}\left(\frac{\epsilon_F}{\epsilon_1}\right)^{2}\hat{j}_0,\\
\frac{d\boldsymbol{j}^e_{d}}{dt}+\frac{d\boldsymbol{j}^e_{\text{ex}}}{dt}+\frac{d\boldsymbol{j}^h_{d}}{dt} &\sim -\frac{D}{4\pi}\left(\frac{\epsilon_F}{\epsilon_1}\right)^{5/2}\hat{j}_0,\\
\frac{d\boldsymbol{j}^h_{\text{ex}}}{dt} &\approx -\frac{D}{9}\left(\frac{\epsilon_F}{\epsilon_1}\right)^{3/2}\hat{j}_0.
\end{aligned} \tag{E14}$$

Calculating the rate of change of the total current, we then get for the asymptotic behavior in the limit $\epsilon_F \ll \epsilon_1$

$$\begin{aligned}
\frac{d\boldsymbol{j}^{(\text{tot})}}{dt} &= \frac{d\boldsymbol{j}^e_{d}}{dt}+\frac{d\boldsymbol{j}^e_{\text{ex}}}{dt}+\frac{d\boldsymbol{j}^h_{d}}{dt}-\left(\frac{d\boldsymbol{j}^e_{\text{inter}}}{dt}+\frac{d\boldsymbol{j}^h_{\text{inter}}}{dt}\right)+\frac{d\boldsymbol{j}^h_{\text{ex}}}{dt}\\
&\approx \frac{d\boldsymbol{j}^h_{\text{ex}}}{dt}+\mathcal{O}\left[\left(\frac{\epsilon_F}{\epsilon_1}\right)^2\right]\\
&\approx -\frac{D}{9}\left(\frac{\epsilon_F}{\epsilon_1}\right)^{3/2}\hat{j}_0+\mathcal{O}\left[\left(\frac{\epsilon_F}{\epsilon_1}\right)^2\right].
\end{aligned} \tag{E15}$$

[1] K. S. Novoselov, D. Jiang, F. Schedin, T. J. Booth, V. V. Khotkevich, S. V. Morozov, and A. K. Geim, Proc. Natl. Acad. Sci. USA **102**, 10451 (2005).

[2] C. L. Kane and E. J. Mele, Phys. Rev. Lett. **95**, 146802 (2005).

[3] M. König, S. Wiedmann, C. Brüne, A. Roth, H. Buhmann, L. W. Molenkamp, X.-L. Qi, and S.-C. Zhang, Science **318**, 766 (2007).

[4] A. H. Castro Neto, F. Guinea, N. M. R. Peres, K. S. Novoselov, and A. K. Geim, Rev. Mod. Phys. **81**, 109 (2009).

[5] L. Fu and C. L. Kane, Phys. Rev. B **76**, 045302 (2007).

[6] D. Hsieh, D. Qian, L. Wray, Y. Xia, Y. S. Hor, R. J. Cava, and M. Z. Hasan, Nature (London) **452**, 970 (2008).

[7] M. Z. Hasan and C. L. Kane, Rev. Mod. Phys. **82**, 3045 (2010).

[8] X.-L. Qi and S.-C. Zhang, Rev. Mod. Phys. **83**, 1057 (2011).

[9] A. H. MacDonald, Nat. Mater. **11**, 409 (2012).

[10] F. Bonaccorso, Z. Sun, T. Hasan, and A. C. Ferrari, Nat. Photon. **4**, 611 (2010).

[11] D. Kong and Y. Cui, Nat. Chem. **3**, 845 (2010).

[12] J. Park, Y. H. Ahn, and C. Ruiz-Vargas, Nano Lett. **9**, 1742 (2009).

[13] J. W. McIver, D. Hsieh, H. Steinberg, P. Jarillo-Herrero, and N. Gedik, Nat. Nanotech. **7**, 96 (2011).

[14] C. Kastl, T. Guan, X. Y. He, K. H. Wu, and Y. Q. Li, Appl. Phys. Lett. **101**, 251110 (2012).

[15] D. Sun, C. Divin, M. Mihnev, T. Winzer, E. Malic, A. Knorr, J. E. Sipe, C. Berger, W. A. de Heer, P. N. First *et al.*, New J. Phys. **14**, 105012 (2012); see also M. Mittendorff, T. Winzer, E. Malic, A. Knorr, C. Berger, W. A. de Heer, H. Schneider, M. Helm, and S. Winnerl, Nano Lett. **14**, 1504 (2014).

[16] M. Freitag, T. Low, W. Zhu, H. Yan, F. Xia, and P. Avouris, Nat. Commun. **4**, 1951 (2013).

[17] A. Junck, G. Refael, and F. von Oppen, Phys. Rev. B **88**, 075144 (2013).

[18] V. V. Cheianov and V. I. Fal'ko, Phys. Rev. Lett. **97**, 226801 (2006).

[19] S. Butscher, F. Milde, M. Hirtschulz, E. Malic, and A. Knorr, Appl. Phys. Lett. **91**, 203103 (2007).

[20] T. Stauber, N. M. R. Peres, and F. Guinea, Phys. Rev. B **76**, 205423 (2007).

[21] W.-K. Tse and S. Das Sarma, Phys. Rev. B **79**, 235406 (2009).

[22] T. Winzer, A. Knorr, and E. Malic, Nano Lett. **10**, 4839 (2010).

[23] R. Kim, V. Perebeinos, and P. Avouris, Phys. Rev. B **84**, 075449 (2011).

[24] T. Winzer and E. Malić, Phys. Rev. B **85**, 241404 (2012).

[25] J. C. W. Song, K. J. Tielrooij, F. H. L. Koppens, and L. S. Levitov, Phys. Rev. B **87**, 155429 (2013).

[26] A. Tomadin, D. Brida, G. Cerullo, A. C. Ferrari, and M. Polini, Phys. Rev. B **88**, 035430 (2013).

[27] D. Hsieh, F. Mahmood, J. W. McIver, D. R. Gardner, Y. S. Lee, and N. Gedik, Phys. Rev. Lett. **107**, 077401 (2011).

[28] N. Kumar, B. A. Ruzicka, N. P. Butch, P. Syers, K. Kirshenbaum, J. Paglione, and H. Zhao, Phys. Rev. B **83**, 235306 (2011).

[29] M. Breusing, S. Kuehn, T. Winzer, E. Malić, F. Milde, N. Severin, J. P. Rabe, C. Ropers, A. Knorr, and T. Elsaesser, Phys. Rev. B **83**, 153410 (2011).

[30] J. A. Sobota, S. Yang, J. G. Analytis, Y. L. Chen, I. R. Fisher, P. S. Kirchmann, and Z.-X. Shen, Phys. Rev. Lett. **108**, 117403 (2012).

[31] M. Hajlaoui, E. Papalazarou, J. Mauchain, G. Lantz, N. Moisan, D. Boschetto, Z. Jiang, I. Miotkowski, Y. P. Chen, A. Taleb-Ibrahimi *et al.*, Nano Lett. **12**, 3532 (2012).
[32] S. Tani, F. Blanchard, and K. Tanaka, Phys. Rev. Lett. **109**, 166603 (2012).
[33] I. Gierz, J. C. Petersen, M. Mitrano, C. Cacho, I. C. E. Turcu, E. Springate, A. Stör, K. Axel, U. Starke, and A. Cavalleri, Nat. Mater. **12**, 1119 (2013).
[34] D. Brida, A. Tomadin, C. Manzoni, Y. J. Kim, A. Lombardo, S. Milana, R. R. Nair, K. S. Novoselov, A. C. Ferrari, G. Cerullo, and M. Polini, Nat. Commun. **4**, 1987 (2013).
[35] J. C. W. Song, M. S. Rudner, C. M. Marcus, and L. S. Levitov, Nano Lett. **11**, 4688 (2011).
[36] M. Müller and S. Sachdev, Phys. Rev. B **78**, 115419 (2008).
[37] C.-X. Liu, X.-L. Qi, H. J. Zhang, X. Dai, Z. Fang, and S.-C. Zhang, Phys. Rev. B **82**, 045122 (2010).
[38] D. Greenaway and G. Harbeke, J. Phys. Chem. Solids **26**, 1585 (1965).
[39] V. Sandomirsky, A. V. Butenko, R. Levin, and Y. Schlesinger, J. Appl. Phys. **90**, 2370 (2001).
[40] The total scattering rate Γ actually diverges for a perfectly linear dispersion. As this divergence is due to almost collinear scattering, it only affects the total scattering rate. The rate of change of the current remains always well defined. In Fig. 1, the divergence of Γ is regularized by the physical particle-hole asymmetry. For perfectly linear dispersion, the divergence could also be regularized by dynamic screening within the random phase approximation [25, 26].
[41] For certain 1D systems, equilibration between left and right movers can be remarkably slow; see T. Karzig, L. I. Glazman, and F. von Oppen, Phys. Rev. Lett. **105**, 226407 (2010).
[42] J. C. W. Song (private communication).